NJC

Accepted Manuscript

This is an *Accepted Manuscript*, which has been through the Royal Society of Chemistry peer review process and has been accepted for publication.

Accepted Manuscripts are published online shortly after acceptance, before technical editing, formatting and proof reading. Using this free service, authors can make their results available to the community, in citable form, before we publish the edited article. We will replace this *Accepted Manuscript* with the edited and formatted *Advance Article* as soon as it is available.

You can find more information about *Accepted Manuscripts* in the Information for Authors.

Please note that technical editing may introduce minor changes to the text and/or graphics, which may alter content. The journal's standard Terms & Conditions and the Ethical guidelines still apply. In no event shall the Royal Society of Chemistry be held responsible for any errors or omissions in this *Accepted Manuscript* or any consequences arising from the use of any information it contains.

ROYAL SOCIETY OF CHEMISTRY

www.rsc.org/njc

Cite this: DOI: 10.1039/c0xx00000x

www.rsc.org/xxxxxx

ARTICLE TYPE

Multifaceted core-shell nanoparticles: superparamagnetism and biocompatiblity

Debasmita Sardar,[a,b] S. K. Neogi,[b,c] S. Bandyopadhyay,[b,c] Biswarup Satpati,[d] Manisha Ahir,[b] Arghya Adhikary,[b] Ruchi Jain,[e] Chinnakonda S. Gopinath[e] and Tanushree Bala[a,b*]

Received (in XXX, XXX) Xth XXXXXXXXX 20XX, Accepted Xth XXXXXXXXX 20XX

DOI: 10.1039/b000000x

Abstract: $Ni_{core}Ag_{shell}$ nanoparticles were synthesized by redox transmetallation reaction. Reduction potential match was encouraging to attempt the synthesis of $Ni_{core}Au_{shell}$ system too. However, it could be achieved only after an effective surface modification on Ni-core. Thorough characterizations (UV-Vis spectroscopy, Fluorescence spectroscopy, XRD, XPS, FTIR, TEM, EDX) proved the necessity of surface modification and the success of synthesis of both types of core-shell structures. The chemical composition and topography were determined using STEM-HAADF analysis and EFTEM imaging. Fourier transform infrared (FTIR) spectroscopy confirmed the surface modification of Ni nanoparticles and the interactions involved between the ligands and metals (in core and/or shell) at various steps of the synthetic process. Even after the formation of noble metal shell the magnetic core was found to retain its superparamagnetic nature. On addition, Au-shell protected the core from aerial oxidation and decreased toxicity as compared to pristine Ni nanoparticles as observed by MTT assay on normal cells (PBMC).

1. Introduction:

It is well known that materials in nano-scale domain exhibit very unique electronic,[1] optical,[2] magnetic[3] properties which their bulk counterparts[4] cannot achieve. Among assorted nanomaterials, the magnetic metallic nanoparticles can provide high magnetic moment[5] which is useful in ferrofluids, magnetic carriers for targeted drug delivery, magnetic data storage and cell separation. Various medical applications such as biosensors,[6] hyperthermia of tumours,[7] targeted drug delivery,[8] ultra sensitive disease detection, DNA separation, [9] and magnetic resonance imaging (MRI)[10] can also be initiated with magnetic nanoparticles, provided cytotoxicity of the materials used for biological purposes is low enough. Though researchers have achieved shape and size selectivity for these kinds of particles, the instability of magnetic metals and their high cytotoxicity are still considered to be active issues to work on. The naturally occurring high moment magnetic metals like Fe, Co, Ni are very prone towards aerial oxidation.[11] Thus there is an earnest need to impart better stability without sacrificing their magnetic properties. Enveloping the magnetic core with a shell of noble metal is an innovative avenue to achieve the goal. Sincere efforts have been observed for the synthesis of multicomponent hybrid nanomaterials in form of core-shell or nanoalloy over the past few years.[12-14] Magnetic-core noble metal-shell[15,16] can definitely be considered as the kingpin of this domain. Synthesis of such structures offers few hurdles mainly because of the abrupt crystal lattice mismatch between magnetic metal and noble metal. Secondly, imparting the stability of the magnetic core turns to be difficult when the core comprises of pure magnetic metal (e.g. Ni, Co, Fe) in comparison to oxides (e.g. Fe_2O_3 or Fe_3O_4). On the other hand, once synthesized, such hybrid system can pertain superparamagnetism of the core and distinct optical properties of the shell (Ag, Au), making them lucrative as multifunctional materials due to such synergistic effect. It is interesting to note here among several choice of noble metals, Au has been largely selected as shell forming material, followed by Ag. Gold coating ensures stability as well as bio compatibility of the hybrid. Specific surface functionalization with biocompatible proteins can also be initiated for such nanohybrids.[17]

A number of techniques have been administered for the production of such nanohybrids : thermal evaporation,[18] sol-gel method,[19] epitaxial method,[20] co-precipitation,[21] hydrothermal,[22] water-oil microemulsion,[23] pulsed laser ablation,[24] reverse micelle method[25] are few to mention. Apart from these, redox-transmetallation process[26] has also been aimed to synthesize magnetic-core noble metal-shell. It has several benefits compared to well-practiced sequential reduction techniques: (1) no need of an added reducing agent for the shell formation, (2) site selective spontaneous reduction of the precursors used for shell formation, without any self-nucleation. However, transmetallation route is definitely not full-proof process for making such magnetic-core noble metal-shell structures, limitations may always creep in. Firstly the choice of the core-shell pair is restricted since proper matching of the reduction potential of the duo is the prime requirement for this reaction. Moreover the surface potential and surface capping of the core materials should solicit the approach of the secondary precursors. Lu *et al.* have shown PVP capping can render the surface positively charged for 112 nm Co-core synthesized in water, which facilitates the electrostatic absorption

of a gold salt [$AuCl_4^-$] and hence the formation of Co-Au yolk/shell nanohybrids.[27] Thus alteration of surface potential or changing the secondary precursor in form of suitable compounds is common routes to assist transmetallation. E.g. Bao *et al.* have followed transmetallation using [$(C_6H_5)3P$]AuCl as gold precursor, the solvent chosen are DCB, toluene.[28]

In this paper we report the synthesis of stable nickel nanoparticles in aqueous medium followed by their conversion to $Ni_{core}Ag_{Shell}$ and $Ni_{core}Au_{shell}$ nanocomposites. It is expected the secondary precursors Ag^+ and Au^{3+} would act likewise to generate the core-shell structures. It has been observed that $Ni_{core}Ag_{Shell}$ follows the simple transmetallation method owing to their allied reduction potential. Nonetheless, the similar matching of reduction potential between Ni^0 and $AuCl_4^-$ failed to produce $Ni_{core}Au_{shell}$ nanocomposites. Surface modification of Ni-core via an amino acid L-Tryptophan does the trick. An attempt has been made to unfold the reasons via extensive characterizations using UV-Vis spectroscopy, Zeta potential measurement, High Resolution Transmission Electron Microscopy (HRTEM), Fourier Transform Infrared (FTIR) spectroscopy, X-ray diffraction (XRD) and X-ray photoelectron spectroscopy (XPS) for both $Ni_{core}Ag_{Shell}$ and $Ni_{core}Au_{shell}$ nanocomposites. The magnetic property has also been measured using superconducting quantum interference device vibrating sample magnetometer (SQUID-VSM). MTT assay on normal cells (PBMC) have shown reduced toxicity for $Ni_{core}Au_{Shell}$ nanoparticles as compared to Ni, which definitely merits this composite for potential biological applications.

2. Experimental Section:

2.1. Materials:

Nickel nitrate hexahydrate (Ni $(NO_3)_2.6H_2O$), sodium dodecyl sulfate (SDS) ($C_{12}H_{25}NaO_4S$), Oleic acid (9-octadeceonic acid, mentioned as OA throughout the paper)($C_{17}H_{33}COOH$)), silver nitrate ($AgNO_3$), L-Tryptophan ($C_{11}H_{12}N_2O_2$), Gold chloride ($HAuCl_4$) and sodium borohydride ($NaBH_4$) were purchased from Merk, SRL and were utilized as received without further purifications. For biological application culture media RPMI-1640, penicillin, streptomycin, gentamycin, L- glutamine, non-essential amino acids, amphotericin B, MTT [3-(4,5-dimethylthiazol-2- yl)-2,5-diphenyltetrazolium bromide were purchased from HIMEDIA (Mumbai, India). Histopaque-1077 was purchased from Sigma, USA. Fetal bovine serum (FBS) was purchased from Invitrogen (Carlsbad, CA, USA).

2.2. Synthesis of Ni nanoparticles:

In a typical synthesis 10 mL of aqueous solution of $1x10^{-2}$ M nickel nitrate ($Ni(NO_3)_2$) was taken with 10 mL of aqueous solution of $1x10^{-1}$ M sodium dodecyl sulfate (SDS) and 1 mL of methanolic solution of $1x10^{-2}$ M oleic acid. As the total volume of the aqueous solution had to be maintained at 100 mL, volume was made up with double distilled water. Then solid sodium borohydride ($NaBH_4$) was added to initialize the reduction of nickel ions. Immediately as soon as the reducing agent was added the entire solution was turned into black solution. Then the solution was kept in rest at ambient condition for 1 hr. Then the synthesized product was separated into supernatant and pellet by repetitive centrifugation (Relative Centrifugal Force = 6080) at 8000 rpm for 20 mins. After washing the obtained black pellet with deionised water and re-centrifuged with the same water under previous conditions, it was dried in oven for the experiments and further characterization like UV-Vis spectroscopy, FTIR, TEM, XRD, XPS and SQUID-VSM .

2.3. Synthesis of $Ni_{core}Ag_{Shell}$ nanoparticles:

To the diluted Ni nanoparticle solution $1x10^{-2}$ M aqueous $AgNO_3$ solution was added to make the overall concentration of the solution $5x10^{-4}$ M. Then the solution was kept in rest at ambient condition for 1day. After 1 day the solution was again repetitively centrifuged at 8000 rpm for 20 mins for separating the pellet from solution to approach for further characterization like UV-Vis spectroscopy, FTIR, XRD, XPS, TEM and SQUID-VSM.

2.4. Synthesis of $Ni_{core}Au_{Shell}$ nanoparticles:

In this typical reaction, there was a sincere need of Ni-surface modification with 5x10-^{2} M aqueous solution of L-Tryptophan to make the concentration of the overall solution $1x10^{-2}$ M. Detailed characterizations (XRD, UV-Vis spectroscopy, Fluorescence and FTIR) were carried out after this process to observe the surface modification of newly introduced amino acid. To this tryptophan modified Ni nanoparticle solution $1x10^{-1}$ M $HAuCl_4$ solution was added to set the overall concentration of the solution at $1x10^{-3}$ M and was kept at rest for at least 1 day. Then solid sample was collected from the pellet post-centrifugation at 8000 rpm for 20 mins. It was dried thoroughly and used for characterization like UV-Vis, FTIR, TEM, ZETA Potential, XRD , XPS and SQID-VSM.

2.5. Characterization:

UV-Vis Spectroscopy: UV-Vis spectra were recorded by Perkin-Elmer 25 Lambda UV-Vis Spectrometer to monitor the optical properties of Ni_{core}, $Ni_{core}Ag_{shell}$, Trp modified Ni nanoparticle and $Ni_{core}Au_{shell}$ nanoparticles solutions at a resolution of 1nm.

Fluorescence Spectroscopy: Fluorescence spectra was analyzed at room temperature by Perkin-Elmer LS55 fluorimeter fitted with a 450 W xenon arc lamp, using 6 nm slits for both excitation and emission. A 1 cmexcitation and emission path length quartz cell was used for all of the fluorescence measurements for checking the fluorescence property of trp modified Ni nanoparticles and thus for $Ni_{core}Au_{shell}$ nanoparticles.

Zeta Potential: Zeta potential were evaluated by Beckman COULTER Delsa^{TM} NANO C particle analyzer to measure the zeta potential at surface of three solutions at different steps.

Fourier Transform Infrared Spectroscopy: Fourier Transform Infrared (FTIR) spectroscopy were measured by Perkin-Elmer FTIR spectrometer at a resolution of 4 cm^{-1} to evaluate the bonding interaction at different steps after mixing the powder samples with solid potassium bromide. The FTIR spectrum of

pure SDS, Oleic Acid and L-Tryptophan was recorded for comparison.

Transmission Electron Microscopy: Transmission electron microscopy (TEM) investigations were carried out using FEI, T-F30, S-T microscope operating at 300 kV. High-angle annular dark field scanning transmission electron microscopy (STEM-HAADF) which is employed here using the same microscope, equipped with a scanning unit and a HAADF detector from Fischione (model 3000). The compositional analysis was performed by energy dispersive X-ray spectroscopy (EDS, EDX Inc.) attachment on the TF30. Energy-filtered TEM (EFTEM) measurements were carried out using GIF Quantum SE (model 963). Samples for these purposes are prepared by simple drop casting the solution on carbon coated copper grid and allowing the solutions to dry up.

X-ray Photoelectron Spectroscopy: X-ray photoelectron spectra (XPS) of the catalysts were recorded with custom built ambient pressure photoelectron spectrometer (APPES) (Prevac, Poland), equipped with VG Scienta's R3000HP analyzer and MX650 monochromator[29,30] Monochromatic Al Kα X-ray was generated at 450 W and used for measuring X-ray photoelectron spectrum (XPS) of the above samples. Base pressure in the analysis chamber was maintained in the range of 2×10^{-10} Torr. The energy resolution of the spectrometer was set at 0.7 eV at a pass energy of 50 eV. Binding energy (BE) was calibrated with respect to Au $4f_{7/2}$ core level at 84.0 eV. The error in the reported BE values is within 0.1 eV. For peak synthesis, a mixed Gaussian-Lorenzian function with a Shirley type background subtraction was used. Samples were flooded with low energy electrons for efficient charge neutralisation.

X-ray Diffraction: X-ray diffraction pattern of dry sample of Ni, $Ni_{core}Ag_{shell}$, $Ni_{core}Au_{shell}$ nanoparticles were recorded from Bruker D-8 Advance SWAX diffractometer operated at a voltage of 40 kV and a current of 40 mA with Cu Kα radiation.

Magnetic measurement: The magnetic measurements of the sample have been performed by a superconducting quantum interference device vibrating sample magnetometer (SQUID-VSM, Quantum Design). The magnetization measurements dependent on both magnetic field and temperature have been performed. Field dependent magnetization (M-H) measurements of the sample have been made at 300K and 10K. Temperature dependent magnetization (M-T) measurements have been performed at 150 Oe, under zero field cool (ZFC) and field cool (FC) conditions.

2.6. Cytotoxicity analysis:

Peripheral Blood Mononuclear Cells (PBMC) isolation: Human whole blood was collected in heparinized vacutainer blood collection tubes (BD, Franklin Lakes,NJ) from adult healthy volunteers with prior consent. Whole blood (100 ml) was diluted with 150 ml of RPMI-1640 and then layered in centrifuge tubes onto 120 ml of Histopaque-1077 gradient. After centrifugation the peripheral blood mononuclear cells (PBMC) layer was washed twice with PBS and re-suspended followed by culture in RPMI-1640 with 10% FBS.

In-vitro cytotoxicity Assay: MTT [3-(4,5-dimethylthiazol-2- yl)-2,5-diphenyltetrazolium bromide] assay was performed on Peripheral Blood Mononuclear Cells (PBMC) using different concentrations of Ni and $Ni_{core}Au_{Shell}$ nanoparticles to check the toxicity of the nanocarrier. The cells were seeded in a 24 well plates at a density of $5x10^4$ cells/ml in each well and allowed to adhere for 24 h. The cells were incubated for 24 h with different concentration of Ni and Ni-Au followed by incubation in media containing 0.5 mg mL 1 of MTT for 3–4 h at 37 ˚C. The resulting formazan crystals were dissolved in an MTT solubilization buffer and the absorbances were measured at 570 nm by using a UV/Vis/NIR Spectrophotometer (Perkin Elmer, Waltham, MA, USA) and the values were compared to the control cells.

3. Results and discussion:

Ni nanoparticles prepared by the above mentioned technique were capped by oleic acid and SDS. These particles were highly stable in aqueous medium against oxidation and precipitation. It could be preserved for long time in the aqueous dispersion at room temperature as well as in the powder form. The conversion of pure Ni to $Ni_{core}Ag_{shell}$ system was accomplished by a simple transmetallation reaction. This reaction occurred since the reduction potentials of $Ni^{2+} + 2e \rightarrow Ni^0$ (- 0.23 V) and $Ag^+ + e \rightarrow Ag^0$ (+ 0.80 V) were such that $Ni^0 + 2Ag^+ \rightarrow Ni^{2+} + 2Ag^0$ was a spontaneous reaction and thus simple mixing of Ag^+ precursors with Ni nanoparticles solution resulted in $Ni_{core}Ag_{shell}$ system capped by oleic acid. Thus the outer layers of Ni atoms in Ni nanoparticles acted as sacrificial agent for the reduction of Ag^+ to Ag^0.

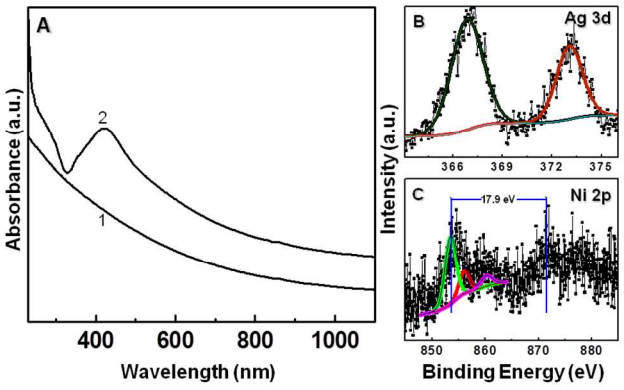

Fig. 1 (A) UV-VIS absorption spectra of aqueous solution of Ni nanoparticle (Curve 1) and $Ni_{core}Ag_{shell}$ nanoparticle (Curve 2). XPS analysis for Ag 3d (B) and Ni 2p (C) as obtained from $Ni_{core}Ag_{shell}$ nanoparticles.

The formation of Ag shell was validated by UV-Vis spectroscopy, Fig. 1A. The UV-Vis spectrum of the pristine oleic acid capped Ni nanoparticles (Curve 1, Fig. 1A) was almost featureless with a monotonic increase in the absorbance with decrease in wavelength and agreed well with those reported for

Ni nanoparticles. The development of a broad surface plasmon resonance peak at 420 nm (Curve 2, Fig. 1A) after the addition of aqueous $AgNO_3$ to Ni nanoparticles was attributed to metallic silver in the nanoscale regime.[15,16] XPS results supported the same, showing Ag $3d_{5/2}$ and $3d_{3/2}$ spin orbit core levels (Fig. 1B) of $Ni_{core}Ag_{shell}$ nanoparticles centered at 372.9 eV and 366.9 eV BE with a energy gap of 6.0 eV between them. This undoubtedly corresponded to Ag^0 state.[31] XPS signature of Ni $2p_{3/2}$ (Fig. 1C) from core could be fitted into three significant components: the major component at 853.6 eV along with a minor one at 856.2 eV.[32] The third peak at 860.4 eV was the satellite peak for Ni 2p. The major component was plausibly due to Ni^0 oxidation state, where as the minor one could be due to oxides or the Ni bound to the –COOH group of the oleic acid. The Ni $2p_{1/2}$ spin orbit core level was found at 871.5 eV, the separation being 17.9 eV. The overall signal of Ni 2p spectra of $Ni_{core}Ag_{shell}$ nanoparticle was found to be weak and associated with high background. This was attributed to the presence of Ni within the photoelectron escape (or probing) depth of 5 nm, with Ag-layers on the top of Ni layers. The electrons released from Ni-core suffered more collisions than the electrons from Ag-shell, and the high background observed in Ni 2p core level was rather very natural for the element which was enveloped by another.[33] XPS was also recorded from pristine Ni nanoparticles for comparison (Supporting Information SI-1). Here also Ni $2p_{3/2}$ could be fitted into two components having similar positions Fig. 1C (854.87 eV and 860.69 eV). Ni $2p_{1/2}$ was found at a separation of 17.68 eV. The prominent nature of the peak (less noisy) and relatively smooth background definitely distinguish the spectra from that of $Ni_{core}Ag_{shell}$, rather it supported the conclusion drawn from the nature of the curve of Fig. 1C.

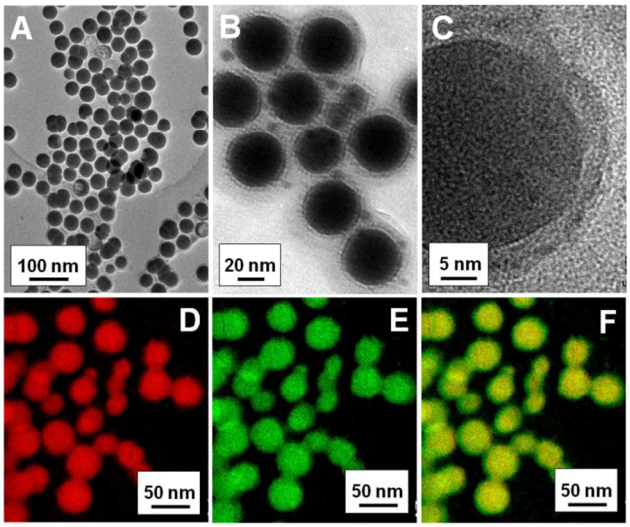

Fig. 2 (A) Transmission electron micrographs of Ni nanoparticle (B) Bright field TEM image of $Ni_{core}Ag_{shell}$ nanoparticle (C) HRTEM image of the same showing the contrast between core (Ni) and shell (Ag). (D, E) EFTEM images corresponding to Ni and Ag respectively showing respective elements in $Ni_{core}Ag_{shell}$ nanoparticles (F) Overlay of Ni – Ag clearly showing the core-shell structure.

The structural information about the $Ni_{core}Ag_{shell}$ was best discerned by TEM, Fig. 2. As prepared Ni nanoparticles were spherical (Fig. 2A) with the average particle size 38.6±2,25 nm as demonstrated by the particle size distribution histogram (Supporting Information SI-2). The transmetallation reaction with Ag^+ and Ni nanoparticles led to the formation of core-shell structures as observed in TEM and HRTEM (Fig. 2B-C). The calculation of the interplanar distance showed a match with fcc Ag (111) plane, the enlarged image of Fig. 2C exhibited the planes prominently (Supporting Information SI-3). EDX spectra obtained from $Ni_{core}Ag_{shell}$ nanoparticles also evidenced clear signature of Ni, Ag. Other elements like Cu, C, etc came from the grid and the capping ligands, (Supporting Information SI-4). Fig. 2D and 2E represented EFTEM images acquired using a slit about 8 eV across Ni M edge (68 eV) and Ag N edge (56 eV) respectively. Composite image of Ag and Ni (Fig. 2F) clearly validated the core-shell formation. The calculated shell thickness matched well with the shell thickness in Fig. 2C which is ~2 nm. XRD analysis on the core-shell particles also confirmed the presence of (111), (200), (220) and (311) planes of fcc Ag, Fig. 3A.

Fig. 3B showed the FTIR analysis of oleic acid capped Ni nanoparticles (Curve 1) and $Ni_{core}Ag_{shell}$ nanoparticles (Curve 2) which had shown the interactions of oleic acid were different in above two cases. The carboxylic acid stretching frequency of pure oleic acid is 1707 cm^{-1} which was shifted to 1636 cm^{-1} in Ni nanoparticles and the band was clearly split into two (1542 and 1622 cm^{-1}) for $Ni_{core}Ag_{shell}$ nanoparticles. The methylene –H band at 2957 cm^{-1} remained unaltered in its position for both. This pointed out, here, plausibly the carboxylic acid group not the double bond interacted with Ni surface for pristine Ni nanoparticles and also with the Ag surface after the formation of Ag-shell.[16]

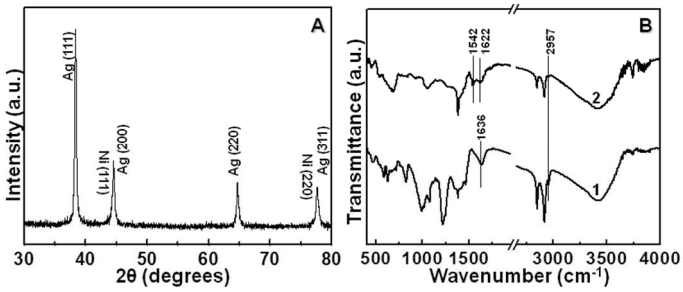

Fig. 3 (A) XRD of $Ni_{core}Ag_{shell}$ nanoparticle (B) FTIR spectra recorded from Ni nanoparticle (Curve 1) and $Ni_{core}Ag_{shell}$ nanoparticle (Curve 2).

Similar attempt was adopted for the synthesis of $Ni_{core}Au_{shell}$ system since the reaction $AuCl_4^- + 3e \rightarrow Au + 4Cl^-$ (+ 0.93 V) also ensured a spontaneous transmetallation with Ni^0 system. Failure to generate $Ni_{core}Au_{shell}$ nanoparticles prompted a detailed investigation of both $Ni_{core}Ag_{shell}$ and $Ni_{core}Au_{shell}$ synthetic strategy and surface composition. Zeta potential measurement on pristine Ni nanoparticles capped with oleic acid was found to be negative (Supporting Information SI-5), which

definitely facilitated the approach of Ag^+ towards the surface of Ni nanoparticles and hence the transmetallation proceeded smoothly. On the other hand $AuCl_4^-$ ions were hindered to reach the surface of these colliodal Ni nanoparticles. Entrenched to this plausible cause, a very simple surface modification was attempted on Ni nanoparticles with L-Tryptophan (Trp). The presence of an indole functional group helped Trp to act basic in aqueous solution of pH 7.22 (this was the pH prevailed in the colloidal solution of Ni nanoparticles). The Zeta potential was found to be nominally negative for Trp modified Ni nanoparticles (Supporting Information SI-6). Conceptually it should again hinder the approach of $AuCl_4^-$ ions. But the advantage of Trp was its ability to reduce $HAuCl_4$ to Au nanoparticles.[34] Thus surface bound Trp helped in the reduction of chloroaurate ions to form Au-shell on Ni nanoparticles. The overall synthetic approach for both $Ni_{core}Ag_{shell}$ and $Ni_{core}Au_{shell}$ system was delineated in Scheme 1.

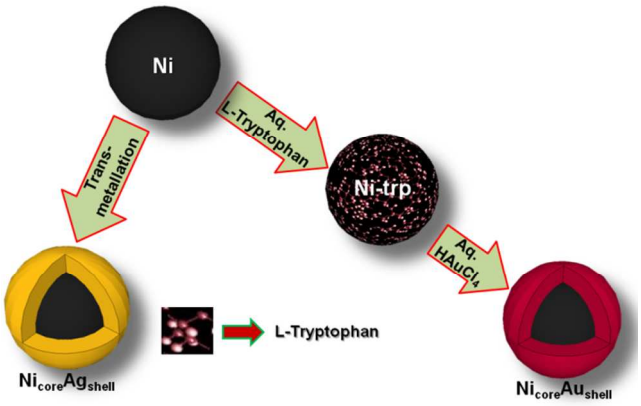

Scheme 1: Schematic representation of different steps involved in the synthesis of $Ni_{core}Ag_{shell}$ and $Ni_{core}Au_{shell}$ nanoparticles.

The incorporation of Trp on Ni surface and its assistance towards reduction of $AuCl_4^-$ were established by a UV-Vis, Fluorescence, XRD and FTIR analyses, Fig. 4. The UV-Vis spectrum of pristine Ni nanoparticles was featureless as expected (Curve 1, Fig. 4A). The incorporation of Trp generated a peak at 279 nm (Curve 2, Fig. 4A) which was characteristic to L-Tryptophan amino acid.[35] After the reduction of $AuCl_4^-$ to Au^0 a broad peak was observed in the region 579 nm indicating the formation of shell/other anisotropic structures for gold (Curve 3, Fig. 4A). This type of SPR peak had already been reported for other type of magnetic metallic core-shell system such as core-shell Fe-Au[36] and Co-Au core-shell.[28] Successful surface modification with Trp was also proved from the fluorescence spectra where the peak for Trp was detected at 366 nm after exciting the sample at 279 nm wavelength (Curve 1, Fig. 4B). The intensity of the fluorescence was reduced after the formation of Au^0, again pointing towards the participation of Trp in the process of reduction (Curve 2, Fig. 4B). XRD analysis also substantiated the incorporation of Trp on Ni surface furnishing the diffraction peaks for L-Tryptophan and fcc Ni in Curve 1, Fig. 4C.[37] The peaks for Trp were present in $Ni_{core}Au_{shell}$ XRD pattern which were overlooked by the highly intense peaks of Au (111), Au (200) and Au (220) planes of fcc Au, Curve 2, Fig. 4C. Essential magnification of Curve 2 in the range $2\theta=16^0$-27^0 (Supporting Information SI-7) showed the presence of peaks corresponding to Trp, this ensured the attachment of the amino acid even after the formation of Au-shell.

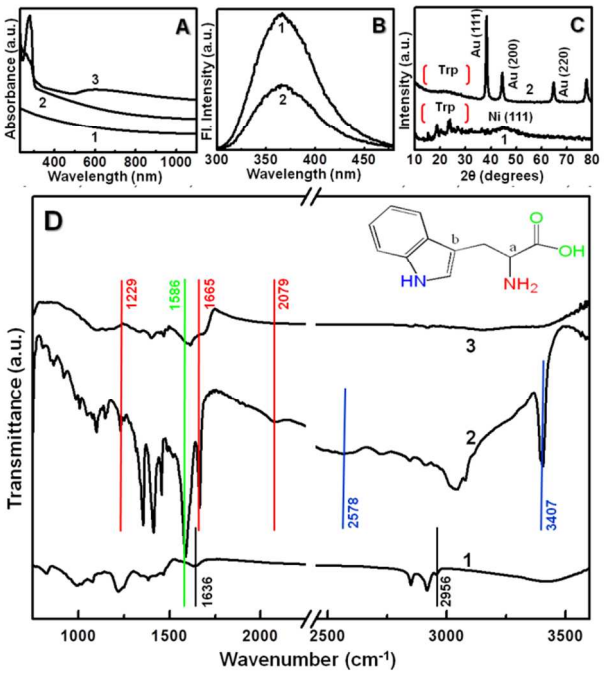

Fig. 4 (A) UV-visible absorption spectra of aqueous solution of Ni nanoparticle (Curve 1), same after modification with Trp (Curve 2), and $Ni_{core}Au_{shell}$ nanoparticle (Curve 3). (B) Fluorescence spectra of Trp modified Ni (Curve 1) and $Ni_{core}Au_{shell}$ nanoparticle (Curve 2) in aqueous medium. (C) XRD of Trp modified Ni (Curve 1) and $Ni_{core}Au_{shell}$ nanoparticle (Curve 2) (D) FTIR spectra recorded from Ni nanoparticle (Curve 1), after surface modification with Trp (Curve 2) and after formation of shell with Au (Curve 3).

Detailed FTIR demonstrated that oleic acid capped Ni nanoparticles gave clear indication of presence of oleic acid, having the relevant bands at 1636 and 2956 cm^{-1} which corresponded to the –COOH group of oleic acid bound to Ni-surface, and the methylene –H, Curve 1, Fig. 4D.[16] The FTIR spectra changed drastically after the interaction with Trp, which was confirmed by the presence of bands characteristic to Trp at 1229, 1586, 1665, 2079, 2578 and 3407cm^{-1} (Curve 2, Fig. 4D). The terminal and indole amine groups ('a' and 'b' as shown in structure of Trp in the inset of Fig. 4D) were found to be relatively free along with a clear shift in asymmetric stretching of the $–COO^-$ group from 1614 cm^{-1} (pure Trp)[38] to 1586 cm^{-1}. This indicated a direct interaction of the carboxylic acid group of Trp to Ni surface, which agreed well with literature reporting a favourable interaction between cobalt/nickel nanoparticles and carboxylic acid group containing ligands.[39] The strong stretching frequency of the terminal amine group at 1665 cm^{-1} was found to

be transformed to a shoulder peak, while the –COO^- stretching at 1586 cm^{-1} was observed to be undisturbed. The signatures of the indole amine group at 2578 and 3407 cm^{-1} were considerably dampened after the reduction of gold, which validated that the reduction was initiated by the amine group of the indole-ring (Curve 3, Fig. 4D).[34]

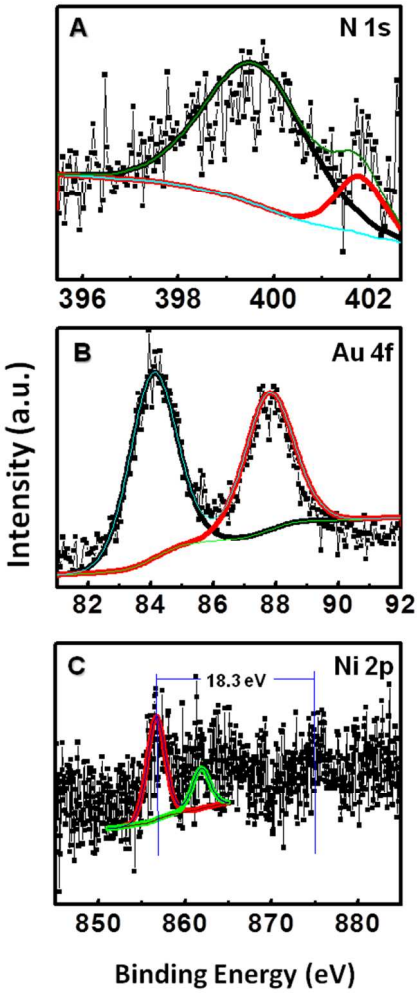

Fig. 5 XPS spectra of (A) N 1s (B) Au 4f (C) Ni 2p from $Ni_{core}Au_{shell}$ nanoparticles.

XPS study also substantiated the fact as mentioned earlier. The presence of well defined N 1s advocated a successful surface modification by Trp. The N 1s spectrum was deconvoluted into two components at binding energies (BE) of 399.4 and 401.7 eV (Fig. 5A). The peak at lower BE corresponds to the first amine group and the higher one to the 2nd amine group, which was attached to the indole ring of Trp. The spectrum of Au $4f_{7/2}$ and $4f_{5/2}$ spin orbit core levels (Fig. 5B) of the $Ni_{core}Au_{shell}$ nanoparticles were observed to be centered at 84.1 eV and 87.8 eV BE, respectively, with an energy gap of 3.7 eV between them. This undoubtedly corresponded to the Au^0 state. This authenticated our proposition of complete reduction of chloroaurate ions in the presence of Trp. The spectrum of Ni was not very clear but could be fitted into two components at 856.62 eV and 861.89 eV respectively, Fig. 5C.[33] The first component was considered as metallic Ni[40] where the 2nd one might arise due to $Ni(OH)_2/Ni_2O_3$. The possibility of adsorbed Ni^{2+}(oleate) complexes on the surface of these nanoparticles could not be ignored, which could also account for the shift to higher BE.[41,42] In comparison to the XPS of Ni 2p from Ni nanoparticles (Supporting Information SI-1), the noisy nature of the curve and high background in Fig. 5C ensured the presence of Ni in the core, away from surface.

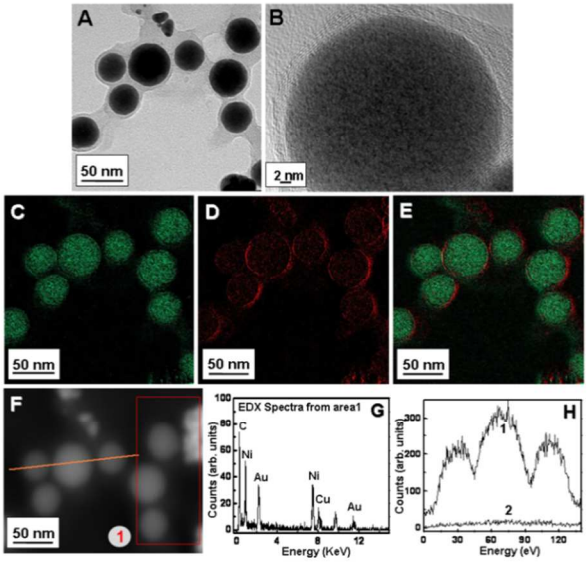

Fig. 6 (A) TEM image of $Ni_{core}Au_{shell}$ nanoparticles (B) HRTEM of a single particle of $Ni_{core}Au_{shell}$. (C, D) EFTEM images corresponding to Ni and Au respectively showing representative elements in $Ni_{core}Au_{shell}$ nanoparticles. (E) Overlay of Ni – Au distinctly showing the core-shell structure. (F) Scanning TEM-HAADF image of $Ni_{core}Au_{shell}$ nanoparticles. (G) EDX spectra obtained from the region marked by a rectangle in previous image. (H) Chemical mapping from the region marked by a straight line in image (F), showing the presence of Ni (Curve 1) and the presence of Au (Curve 2).

Structural information about the core-shell was obtained using TEM, Fig. 6. The high concentration of Ni in the cores and the tendency for Au accretion to form a shell was visible by brightness contrast in TEM image, Fig. 6A. The HRTEM image also (Fig. 6B) envisaged the presence of Au shell very clearly. To investigate the chemical composition of core–shell structure, we performed STEM-HAADF-EDX and EFTEM analysis. Fig. 6C and 6D represents EFTEM images acquired using a slit about 8 eV across Ni M edge (68 eV) and Au O edge (54 eV), respectively. Fig. 6E was the composite image of Au and Ni. The spatial distribution of Ni and Au undoubtedly proved the core-shell structure in this sample. Noticeably in Fig. 6E, the overall size of $Ni_{core}Au_{shell}$ was ~50.2 nm which indicated a clear increase over pristine Ni (estimated to be 38.6 nm, Fig. 2A). It further pointed out to a reduction by Trp on the surface than a transmetallation that operated in case of $Ni_{core}Au_{shell}$ formation. Thus the shell thickness was calculated to be ~5.8 nm. The direct

measurement of shell thickness from Fig. 6E was ~5 nm and in good agreement with the calculated value. STEM-HAADF provided the Z-contrast image, where the intensity of scattered electrons was proportional to the square of the atomic number Z, Fig. 6F. EDX spectrum from area (1) marked in Fig. 6F was plotted in Fig. 6G which clearly proved the presence of Ni and Au. The intense carbon peak cropped up from the organic capping ligands as well as C-coated Cu grid. Cu-signal came from the grid itself. The spatial distributions of atomic contents across the $Ni_{core}Au_{shell}$ nanoparticles were obtained using an Energy Dispersive X-ray spectroscopy (EDX) line profile. Fig. 6H showed the EDX profiles for Ni and Au across the 'line' in Fig. 6F. All these images provided strong concurrent evidence for the successful formation of $Ni_{core}Au_{shell}$ structures by this method.

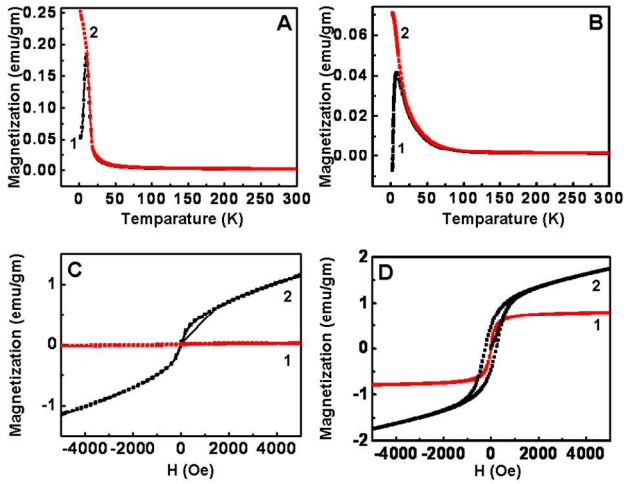

Fig. 7 Temparature dependent magnetization (applied magnetic field = 150 Oe) for zero field cooled measurement (ZFC, Curve 1) and for field cooled measurement (FC, Curve 2) for $Ni_{core}Ag_{shell}$ (A) and also for $Ni_{core}Au_{shell}$ nanoparticles (B). Field dependent magnetization at 300K (Curve 1) and 10 K (Curve 2) for $Ni_{core}Ag_{shell}$ (C) and also for $Ni_{core}Au_{shell}$ nanoparticles (D).

The magnetic characterizations were performed for Ni nanoparticles (Supporting Information SI-8) and the core-shell structures $Ni_{core}Ag_{shell}$ and $Ni_{core}Au_{shell}$, Fig. 7. The temperature dependent magnetization (M-T) measurement for all the particles were carried out at 150 Oe field under zero-field-cooled (ZFC) (Curve 1, Fig. 7A, 7B) and field cooled (FC) (Curve 2, Fig. 7A, 7B) conditions. M-T curves under ZFC and FC conditions diverted from each other at 11K for $Ni_{core}Ag_{shell}$ (Fig. 7A) and at 14K for $Ni_{core}Au_{shell}$ (Fig. 7B) though nature of these curves were almost identical as indicated from Fig. 7A and 7B. These temperatures [11K for $Ni_{core}Ag_{shell}$ and 14K for $Ni_{core}Au_{shell}$] could be considered as the blocking temperature (T_B) for the respective samples. The remarkably sharp blocking temperature transition validated the mono-dispersed nature of the particles as also observed by TEM analysis. Slightly lower T_B for $Ni_{core}Ag_{shell}$ system hinted towards a reduced magnetic core in this case. The blocking temperature of Ni nanoparticles was 18K which agreed well with the literature (Supporting Information SI-8A).[43]

The field dependent magnetization (M-H) measurements for both $Ni_{core}Ag_{shell}$ and $Ni_{core}Au_{shell}$ were performed at temperatures 300K and 10K. It was worthwhile to mention that at 300K, M-H curve of $Ni_{core}Ag_{shell}$ exhibited reversible magnetization as a function of the magnetic field (Curve 1, Fig. 7C) indicating a very weak paramagnetic nature; whereas $Ni_{core}Au_{shell}$ exhibited reversible magnetization as a function of the magnetic field (Curve 1, Fig. 7D) at room temperature 300K. The non-linear nature of this curve particularly in the field range between 500 to 1000 Oe indicated paramagnetism coupled with antiferromagnetism. The saturation in magnetization appeared with a substantially low value and that was another signature of presence of strong antiferromagnetism. Moreover, $Ni_{core}Au_{shell}$ nanoparticles had the tendency to have higher magnetization value at a given field (H, Oe), Fig. 7C and 7D. In case of $Ni_{core}Au_{shell}$ the shell formation was not induced by transmetallation but by the reduction utilizing the surface capping agent Trp. On the other hand, encapsulation by Ag via transmetallation had caused a reduction in the overall magnetic core volume due to partial replacement of surface Ni atoms (Ni^0) with Ag^+. Thus a reduction in magnetic core size might reflect lower magnetization and lower T_B for $Ni_{core}Ag_{shell}$ system, though the decrease was found to be marginal only.[44-46] The alteration in saturation magnetization and blocking temperature would probably become significant with a thicker shell of Au.

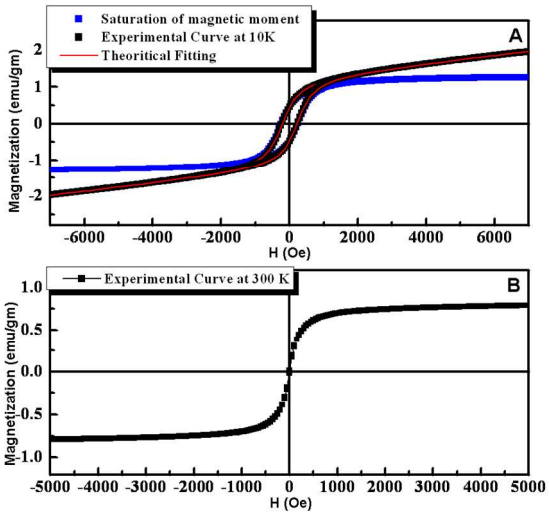

Fig. 8 (A) The solid blue line represents saturation magnetization after the subtraction of the paramagnetic contributions from the experimental data points and the red curve is theoretical fit of the experimental M–H curves. The black line represents the experimental curve at 10K. (B) The experimental curve at 300K for $Ni_{core}Au_{shell}$ nanoparticles.

However, at 10K, the behaviour changed quite drastically. No distinct hyteresis loop was observed for $Ni_{core}Ag_{shell}$ even at 10K (Curve 2, Fig. 7C) and as a whole the curve reflected paramagnetic nature. The M-H curve for $Ni_{core}Ag_{shell}$ at 10K exhibited more linear nature and higher values of magnetization in comparison to M-H curve for $Ni_{core}Au_{shell}$ at 300K. This feature indicated presence of weaker antiferromagnetism in $Ni_{core}Ag_{shell}$ at 10K in comparison to

$Ni_{core}Au_{shell}$ at 300K. So far as M-H curve for $Ni_{core}Au_{shell}$ at 10K was concerned it showed irreversible behaviour with a prominent hysteresis loop (quite strong ferromagnetism) with a substantial coercivity of 239 Oe (Curve 2, Fig. 7D). It further indicated that magnetization was unsaturated (in the field region where there was no irreversibility). It might be due to coexistence of paramagnetic phase along with the ferromagnetic phase.[47] Typically the feature observed in the M-H curves was in accordance with those expected for superparamagnetic nanoparticles. The M-H curves $Ni_{core}Au_{shell}$ at 10K did not fit well with the Brillouin-function as should be the case of purely paramagnetic or ferromagnetic system. But it fitted well with equation (1) given below [47]

$$M(H) = (2M_{FM}^{S}/\pi)\tan^{-1}[(H\pm H_{ci})/H_{ci}\tan\{(\pi M_{FM}^{R})/2 M_{FM}^{S}\}] + \chi H \quad \text{.....(1)}$$

Respaud *et al* [48] described equation (1) consisted of ferromagnetic as well as paramagnetic components where M_{FM}^{S}, M_{FM}^{R}, H_{ci} and χ were saturation magnetization, remanent magnetization the intrinsic coercivity and paramagnetic susceptibility. Subtracting the paramagnetic parts from the experimental data, saturation of magnetization in the field region where there was no irreversibility, could be observed (blue lines, Fig. 8A). The saturation magnetization for $Ni_{core}Au_{shell}$ at 10K was 1.24 emu/g. The strong irreversible magnetic nature at 10K for $Ni_{core}Au_{shell}$ was really noteworthy as evidenced from wide hysteresis loop with substantial coercivity and saturation magnetization values. This kind of nature was absent in case of $Ni_{core}Au_{shell}$ nanoparticles at 300K, Fig. 8B. For non-interacting, randomly oriented, single-domain particles with uniaxial anisotropy, the coercive field H_C (T) at temperature T was found to depend on $H_C(0)$ where $H_C(0) = 0.64\ KM_S^{-1}$ where M_S = saturation magnetization and K = effective anisotropy, which could be taken as a sum of the magnetocrystalline anisotropy (field required to saturate the magnetization in the hard direction), shape anisotropy, surface anisotropy and so on. The coercive field was directly related to the effective anisotropy field; the increase in the coercive field thus clearly signatured enhanced anisotropy in $Ni_{core}Au_{shell}$ system.[49,50] The nature of the M-H curves at 300K and 10K and the saturation magnetization for pure Ni sample also showed good agreement with literature (Supporting Information SI-8B).[43] The low saturation magnetization generally improved further on controlled heating under nitrogen atmosphere as reported earlier for pure Ni due to improved crystallinity.[43]

Study of In-vitro cytotoxicity of nanoparticles on normal human blood cells (PBMC): The MTT assay was performed in order to assess the cytotoxicity of Ni and Ni-Au on peripheral blood mononuclear cells (PBMC). Interestingly our observations revealed that the percentage of PBMC cell survival as assessed by MTT assay was significantly higher upto a certain dose of 200 µg/ml when subjected to Ni and $Ni_{core}Au_{shell}$ nanoparticle exposure respectively (Fig. 9A and 9B). Furthermore, it was observed that the cell survival percentage was found to be decreasing from the dose of 300 µg/ml in case of Ni treated cells. On the contrary, $Ni_{core}Au_{shell}$ nanoparticle caused a decrease in the percentage of PBMC cells viability at a much higher dose i.e from 600µg/ml. These findings thereby established the fact that the Ni showed prominent cytotoxicity in normal cells (PBMC) at a dose considerably lower than the $Ni_{core}Au_{shell}$ nanoparticle. Ni nanoparticle could be much more toxic to normal cells while a shell of Au could enhance biocompatibility to a significant extent, the inception was encouraging enough to test for detailed biocompatibility of $Ni_{core}Au_{shell}$ nanoparticles which will be addressed in future.

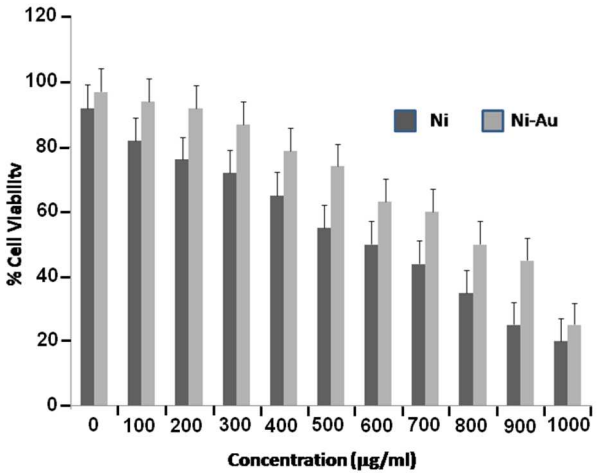

Fig. 9 In-vitro cytotoxicity assay on PBMC cells. Analysis of percentage of cell survival by MTT assay on PBMC at different doses of Ni (A) and $Ni_{core}Au_{shell}$ nanoparticle (B) after 24h of incubation.

Conclusions:

Hetero-structured $Ni_{core}Ag_{shell}$ nanoparticles were synthesized via redox transmetallation on extremely monodispersed colloidal Ni nanoparticles. Prophetic prediction was stipulated for similar synthesis of $Ni_{core}Au_{shell}$ nanoparticles also, via redox transmetallation method. The nature of colloidal Ni surface discriminated between the chosen precursors for Ag-shell and Au-shell, which compelled a surface modification of colloidal Ni by an amino acid to achieve the goal of $Ni_{core}Au_{shell}$ synthesis. This trivial trick helped to overcome the hurdle to generate $Ni_{core}Au_{shell}$ nanoparticles with the most common gold precursor $HAuCl_4$ in aqueous medium at ambient temperature without using any toxic chemicals. This definitely encouraged for further utilization of these particles for biological system. Magnetic measurement (using SQUID-VSM) ensured the retention of the magnetic characteristic of Ni-core where as the noble metal shell imparted the necessary stability for Ni-core which was otherwise prone towards aerial oxidation. Moreover Au-shell reduced the cytotoxicity to a significant extent which is inspirational for further effort in this direction.

Acknowledgements:

TB acknowledges financial support (Project No. Conv/162/Nano Pr 2011) from the Centre for Research in Nanoscience and Nanotechnology (CRNN), University of Calcutta. DS and RJ

acknowledge CRNN and CSIR, respectively, for research fellowship. CSG acknowledges the partial financial support from CSC0404.

Notes and references

[a]Department of Chemistry, University of Calcutta, 92 A.P.C. Road, Kolkata: 700009, India
[b]CRNN, University of Calcutta, JD 2, Sector III, Salt Lake, Kolkata: 700098, India
[c]Department of Physics, University of Calcutta, 92 A.P.C. Road, Kolkata: 700009, India
[d]Surface Physics Division, Saha Institute of Nuclear Physics, 1/AF Bidhannagar, Kolkata-64, India
[e]Catalysis Division and Center of Excellence on Surface Science, CSIR – National Chemical Laboratory, Dr. Homi Bhabha Road, Pune -411 008, India

*To whom correspondence should be addressed: E-mail: tanushreebala@gmail.com

† **Electronic supplementary information (ESI) available:** XPS of pristine Ni nanoparticles (SI-1), Particle size distribution of Ni nanoparticles (SI-2), Magnified HRTEM of $Ni_{core}Ag_{shell}$ (SI-3), EDX spectra of $Ni_{core}Ag_{shell}$ nanoparticle (SI-4), Zeta potential measurement data for Ni (SI-5), Zeta potential measurement data for Trp modified Ni (SI-6), XRD of $Ni_{core}Au_{shell}$ nanoparticles (SI-7) and Magnetic measurement for Ni nanoparticles (SI-8). See DOI: XXXXXXX

References:

1 D. Jariwala, V. K. Sangwan, L. J. Lauhon, T. J. Marksab and M. C. Hersam, *Chem. Soc. Rev*., 2013, **42**, 2824.
2 M. P. Pileni, *New J. Chem.,* 1998, 693.
3 L. M. Rossi, N. J. S. Costa, F. P. Silva and R. Wojcieszak, *Green Chem*., 2014, **16**, 2906.
4 Niemeyer, C. M., Angew. Chem., Int. Ed., 2001, **40**, 4128.
5 J. Bai and J-P Wang, *APPLIED PHYSICS LETTERS*, 2005, **87**, 152502.
6 R. Villalonga, M. L. Villalonga, P. Díeza and J. M. Pingarrón, *J. Mater. Chem*., 2011, **21**, 12858.
7 H. S. Huang and J. F. Hainfeld, *International Journal of Nanomedicine*, 2013, **8**, 2521.
8 B. Chertok, B. A. Moffat, A. E. David, F. Yu, C. Bergemann, B. D. Ross and V. C. Yang, *Biomaterials*, 2008, **29**, 487.
9 Z. M. Saiyed, C. N. Ramchand and S. D. Telang, *J. Phys.: Condens. Matter*, 2008, **20**, 204153.
10 T. D. Schladt, K. Schneider, H. Schild and W. Tremel , *Dalton Trans.,* 2011, **40**, 6315.
11 T. Hyeon, *Chem. Commun..,* 2003, 927.
12 G. Chen, H. Ågren, T. Y. Ohulchanskyya and P. N. Prasad, *Chem. Soc. Rev.,* 2014, DOI: 10.1039/c4cs00170b
13 H-L Jiang and Q. Xu, *J. Mater. Chem.,*2011, **21**, 13705.
14 B.Panigrahy and D. D. Sarma, *RSC Adv*., 2015, **5**, 8918.
15 T. Bala, S. D. Bhame, P. A. Joy, B. L. V. Prasad and M. Sastry, *J . Mater. C hem.*, 2004 , **14** , 2941.
16 T. Bala, S. K Arumugam, R. Pasricha, B. L. V. Prasad and M. Sastry, *J. Mater. Chem.,* **2004**, **14**, 1057.
17 I. Robinson, L. D. Tung, S. Maenosono, C. Wälti and N. T. K. Thanh, *Nanoscale*, 2010, **2,** 2624.
18 H. Liu, Z. Huang, J. Huang, M. Fang, Y-g Liua and X. Wua, *J. Mater. Chem. C*, 2014, **2**, 7761.
19 L. Wang, M. Lu, Y. Liu, J. Li, M. Liu and H. Li, *Ceramint*, 2015, **41**, 4176.
20 M. Tsuji, K. Ikedo, M. Matsunaga and K. Uto, *CrystEngComm*., 2012, **14**, 3411.
21 Y. Il Kim, D. Kim and C. S. Lee, *Physica B*, 2003, **337**, 42.
22 W. Shi, S. Songa and H. Zhang, *Chem. Soc. Rev*., 2013, **42**, 5714.
23 K. A. Dahlberg and J. W. Schwank, *Chem. Mater*. 2012, **24**, 2635.
24 Z. Yan, R. Bao and D. B. Chrise, *Phys. Chem. Chem. Phys*., 2013, **15**, 3052.
25 Chao Liu, Bingsuo Zou, Adam J. Rondinone and Z. John Zhang, *J. Phys. Chem. B,* 2000*,* **104(6)***,* 1141.
26 D. Chen, J. Li, C. Shi, X. Du, N. Zhao, J. Sheng and S. Liu, *Chem. Mater*. 2007**, 19**, 3399.
27 Y. Lu, Y. Zhao, L. Yu, L. Dong, C. Shi, M-J. Hu, Y-J. Xu, L-P Wen and S-H Yu, *Adv. Mater*., 2010, **22**, 1407.
28 Y. Bao, H. Calderon and K. M. Krishnan, *J. Phys.Chem. C,* 2007, **111**, 1941.
29 K. Roy, C. P. Vinod and C. S. Gopinath, *J. Phys. Chem. C* 2013, **117**, 4717.
30 K. Roy and C. S. Gopinath, *Anal. Chem*. 2014, **86**, 3683.
31 N. R Gupta, B. L. V. Prasad, C. S. Gopinath and M. V. Badiger, *RSC. Adv*., 2014, **4**, 10261.
32 S. Velu, K. Suzuki, M. Vijayaraj, S. Barman and C. S. Gopinath, *Appl. Catal. B* 2005, **55**, 287.
33 C.D.W agner, W.M.Riggs, L.E.Da vis, J.F .Moulder , and G.E. Muilenberg, Handbook of X-ray photoelectron spectroscopy, Perkin Elmer Corp., Publishers, Eden Prairie, MN (1979).
34 PR. Selvakannan, S. Mondal, S. Phadtare, A. Gole, R. Pasricha, S. D. Adyanthaya and M. Sastry. *Journal of Colloid and Interface Science,* 2004, **269**, 97.
35 S. W. Lin and T. P. Sakmar, *Biochemistry,* 1996, **35**, 11149.
36 Z. Ban, Y. A Barnakov, F. Li, V. O. Golub and C. J. O'Connor, *J. Mater. Chem*., 2005, **15**, 4660.
37 Y. Li, Y. Zhao and Y. Zhang, *CHIRALITY,* 2015, **27,** 88.
38 Z. Zhengbin, W. Wei, L. Liansheng, F. Youjun and W. Zhijian, *Journal of Colloid and Interface Science,* 1997, **190**, 1
39 N. Wu, L. Fu, M. Su, M. Aslam and K. C. Wong, *Nano Lett.,* 2004, **4**, 383.
40 K.S. Kim and R.E. Davis, *Journal of Electron Spectroscopy*, 1973, **1**, 251.
41 H. Winnischofer, T. C. R. Rocha, W. C. Nunes, L. M. Socolovsky, M. Knobel and D. Zanchet, *ACS Nano*, 2008, **2**, 1313.
42 G. G. Couto, J. J. Klein, W. H. Schreiner, D. H. Mosca, A. J. A. de Oliveira and A. J. G. Zarbin, *J. Colloid Interface Sci*.,2007, **311**, 461
43 D.S. Sidhaye, T. Bala, S. Srinath, H. Srikanth, P. Poddar, M. Sastry and B. L. V. Prasad, *J. Phys. Chem C* 2009, **113,** 3426.
44 P. Poddar, T. T- Shafir, T. Fried and G. Markovich, *Phys. Rev. B*., 2002, **66**, 060403.
45 P. Poddar, H. Srikanth, S. A. Morrison and E. E. Carpenter*, J. Magn. Magn. Mater*. 2005, **288**, 443.
46 P. Poddar, M. B. Morales, N. A. Frey, S. A. Morrison, E. E. Carpenter and H. Srikanth, *J. Appl. Phys*., 2008, **104**, 063901.
47 T. Meron and G. Markovich, *J. Phys. Chem. B*, 2005, **109**, 20232.

48 M. Respaud, J. M. Broto, H. Rakoto, A. R. Fert, L. Thomas, B. Barbara, M. Verelst, E. Snoeck, P. Lecante, A. Mosset,J. Osuna, T. C. Ould, C. Amiens and B. Chaudret, *Phys. Rev.B: Condens. Matter Mater. Phys*., 1998, **57**, 2925.

49 S. Srinath, P. Poddar, R. Das, D. Sidhaye, B. L. V. Prasad, J. Gass and H. Srikanth, *ChemPhysChem*, 2014, **15**, 1619.

50 Y. Sahoo, Y. He, M. T. Swihart, S. Wang, H. Luo, E. P. Furlani and P.N. Prasad, *J. Appl. Phys.,* 2005, **98**, 054308(1-6).

Multifaceted core-shell nanoparticles: superparamagnetism and biocompatiblity

Debasmita Sardar, S. K. Neogi, S. Bandyopadhyay, Biswarup Satpati, Manisha Ahir, Arghya Adhikary, Ruchi Jain, Chinnakonda S. Gopinath and Tanushree Bala*

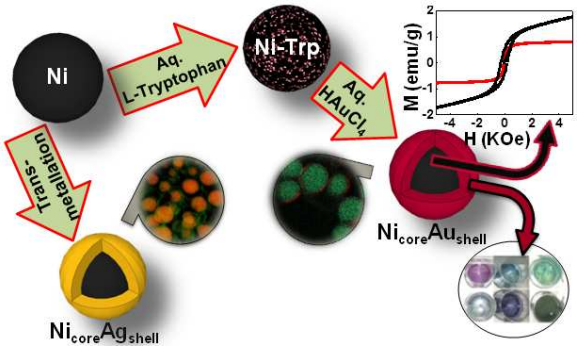

A facile method for synthesis of $Ni_{core}Ag_{shell}$ and $Ni_{core}Au_{shell}$ nanoaprticles with suitable surface modification for the latter has been demonstrated with potential applications.